RESEARCH ARTICLE

Spatiotemporal Patterns and Driving Factors of Vegetation Carbon Sinks at the County Scale in the Chengdu-Chongqing Economic Circle

Wenjing Wang[1], Yuanjie Deng[1,*], Hua'e Dang[1], Yifeng Hai[1], Hang Chen[1], Jincan Chen[1] and Miao Zhang[1]

[1] School of Economics, Sichuan University of Science & Engineering, Zigong 643000, China

Abstract

To address two critical gaps in vegetation carbon sink (VCS) research—its limited policy relevance at the county scale and the insufficient identification of nonlinear interactive effects within driving mechanisms—this study focuses on the Chengdu-Chongqing Economic Circle (CCEC). Using MODIS NPP data (2002–2022), we examined the spatiotemporal dynamics of VCS through time-series analysis, standard deviational ellipse, and spatial autocorrelation analysis. Crucially, we applied the Geodetector model to quantitatively disentangle the roles of natural and anthropogenic drivers. The results show that: (1) VCS followed a fluctuating upward trajectory, peaking in 2019, but declined sharply in 2006 due to an extreme drought; (2) spatially, a "three-belt agglomeration" pattern was identified, with high-value clusters in mountainous areas (Southwestern Sichuan, Southeastern Chongqing, Southeastern Sichuan) and low-value diffusion in plains (Chengdu Plain, Chongqing Valley). The VCS centroid remained consistently located in Anyue County, while spatial clustering gradually weakened; (3) single-factor detection highlighted natural factors—especially elevation ($q > 0.76$)—as dominant drivers of spatial heterogeneity, whereas interaction detection revealed widespread "nonlinear enhancement" between natural and anthropogenic factors. These interactions explained far more variance than individual factors and amplified spatial heterogeneity synergistically. By integrating county-scale analysis with the identification of nonlinear interaction mechanisms, this study provides a scientific foundation for differentiated ecological governance and the precise implementation of China's "Dual Carbon" (carbon peaking and carbon neutrality) goals in the CCEC.

Keywords: Chengdu-Chongqing economic circle (CCEC), vegetation carbon sinks (VCS), county scale, spatiotemporal patterns, geodetector.

Submitted: 23 August 2025
Accepted: 29 August 2025
Published: 01 September 2025

Vol. 1, **No.** 1, 2025.
10.62762/JGEE.2025.856697

***Corresponding author:**
✉ Yuanjie Deng
ecodyj@suse.edu.cn

Citation
Wang, W., Deng, Y., Dang, H., Hai, Y., Chen, H., Chen, J., & Zhang, M. (2025). Spatiotemporal Patterns and Driving Factors of Vegetation Carbon Sinks at the County Scale in the Chengdu-Chongqing Economic Circle. *Journal of Geo-Energy and Environment*, 1(1), 46–60.

1 Introduction

Climate change has become a pressing global challenge, with increasingly severe problems such as frequent extreme weather events, ecosystem degradation, and threats to food security. These challenges have prompted the international community to accelerate climate governance efforts [1]. Enhancing carbon sink capacity—particularly Vegetation Carbon Sinks (VCS)—is a crucial pathway toward achieving carbon neutrality and has become a key indicator of ecosystems' capacity to respond to and regulate climate change [2]. VCS absorb atmospheric CO_2 through photosynthesis and represent one of the most significant potential types of carbon sinks within terrestrial ecosystems. They play a vital role in mitigating greenhouse gas emissions, improving ecological environments, and supporting sustainable development [3, 4]. Therefore, investigating the spatiotemporal evolution of VCS and uncovering their driving mechanisms is essential for advancing China's "Dual Carbon" strategy, enhancing ecosystem carbon sequestration capacity, and formulating sound climate governance policies.

Previous research has extensively examined the estimation, dynamics, and drivers of VCS. On the one hand, remote sensing and modeling approaches have been widely used to characterize spatiotemporal variations of Net Primary Productivity (NPP) and VCS, highlighting the combined influence of natural and anthropogenic factors [5–8]. On the other hand, linear regression and geostatistical models have been applied to identify and quantify the drivers of carbon sinks [9–13]. However, two major gaps remain. First, most studies adopt a grid scale as the analytical unit, while largely overlooking the county scale—a critical spatial unit that directly aligns with policymaking and ecological governance [14]. This omission limits the practical policy relevance of findings. Second, most analyses rely on traditional linear models, with limited application of non-parametric approaches such as the Geodetector, which is specifically designed to identify spatial heterogeneity and factor interactions [15, 16]. This restricts our understanding of the inherent complexity underlying VCS formation. These shortcomings not only reduce the policy applicability of existing research but may also underestimate the deep influence of coupled human–environment processes on VCS dynamics. To address these gaps, it is essential to analyze VCS drivers at the county scale by integrating spatial statistical methods such as the Geodetector. This approach allows for scientific identification of VCS evolution mechanisms under the dual dimensions of natural ecological foundations and anthropogenic interventions.

The CCEC is located at the intersection of the ecological barrier in the upper Yangtze River and China's national urbanization strategy. With complex topography, diverse ecosystem types, and simultaneous pressures from economic development and ecological protection, the CCEC is a critical demonstration zone for exploring pathways of "ecological conservation and green development [17, 18]." Geographically, the region consists of an interlocked distribution of mountains, hills, plains, and basins. Natural terrain and vegetation cover exert strong influences on the spatial distribution of VCS, offering rich potential for analyzing spatial heterogeneity. Meanwhile, counties serve as the fundamental administrative units for resource management and policy implementation, and enhancing their VCS capacity is vital for achieving regional "Dual Carbon" goals. Against this background, this study uses MODIS NPP data (2002–2022), combined with time-series and spatial analysis methods, to systematically characterize the spatiotemporal evolution of VCS at the county scale in the CCEC. Furthermore, the Geodetector is introduced to reveal the roles and interactions of natural and anthropogenic drivers. The findings aim to enrich the multi-scale research framework on carbon sinks and provide both theoretical support and practical guidance for enhancing ecosystem carbon sink functions and implementing differentiated, county-level ecological governance.

2 Data Sources and Research Methods

2.1 Study Area Overview

The CCEC (see Figure 1) is a regional cluster centered on the twin cores of Chengdu and Chongqing[19]. Geographically, it lies between 27°39′–33°02′N and 101°56′–110°12′E, encompassing 15 prefecture-level cities in Sichuan Province (e.g., Chengdu, Zigong, Luzhou) and 29 districts/counties under Chongqing Municipality (e.g., Yuzhong, Wanzhou, Dadukou). The CCEC is located in the core zone of the Sichuan Basin, characterized by pronounced topographic relief. The surrounding areas consist of low mountains and hills (such as the Southwestern Sichuan Mountains and Southeastern Chongqing Mountains) with high vegetation coverage, while the northeastern boundary includes the folded mountain ranges of the Eastern Sichuan Ridge-and-Valley zone. In contrast, densely populated and industrialized urban

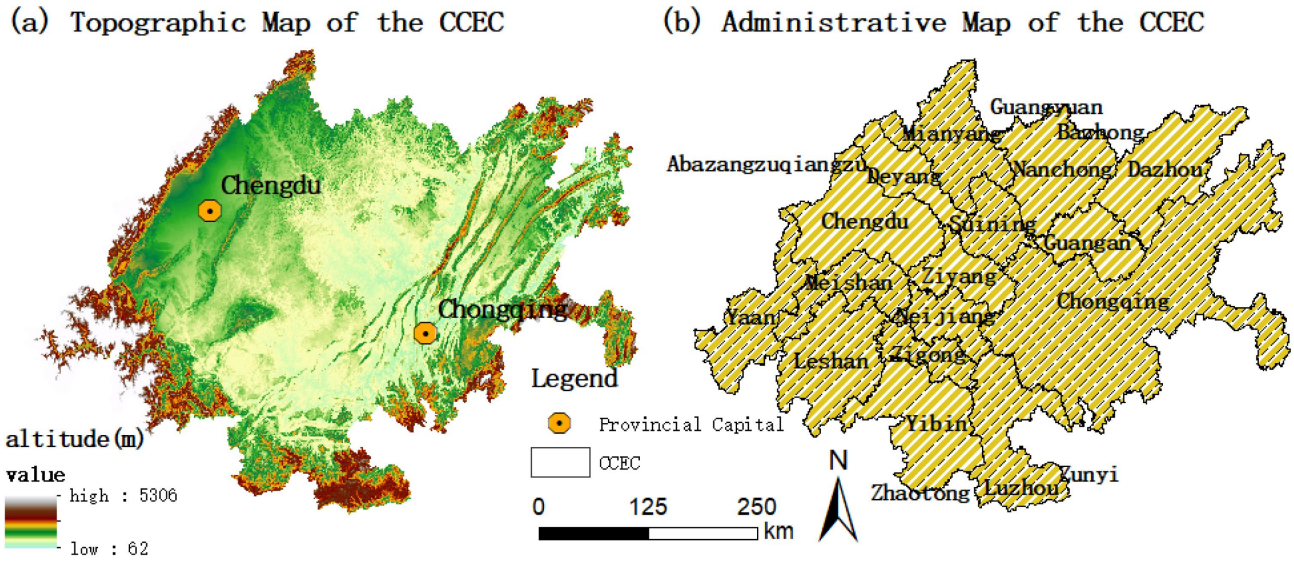

Figure 1. Map of the study area.

cores are concentrated in the Chengdu Plain and the Chongqing Western Valley, which feature plains and shallow hills [20]. This "peripheral mountains–central plains" topographic configuration creates a clear spatial separation between high-VCS zones dominated by natural vegetation and low-VCS zones strongly influenced by human activity. The CCEC also lies at the intersection of the Yangtze River Corridor (horizontal axis) and the Baotou–Kunming Corridor (vertical axis) within China's "Two Horizontal and Three Vertical" national urbanization strategy. As the country's designated "Fourth Growth Pole [21]," the region possesses significant locational advantages, linking east and west as well as north and south. Consequently, the spatiotemporal evolution of VCS in the CCEC provides an important demonstration for both ecological barrier construction in the upper Yangtze River and the advancement of regional "Dual Carbon" goals.

2.2 Data Sources

Vegetation NPP data were obtained from NASA's MOD17A3 product (spatial resolution: 500 m; temporal resolution: annual) and processed through the Google Earth Engine (GEE) platform to generate a 2002–2022 dataset for Sichuan Province. Climatic data, including annual mean temperature and precipitation, were derived from 1 km resolution gridded monthly datasets (1901–2022) provided by the National Tibetan Plateau Data Center (https://data.tpdc.ac.cn/home). Elevation and slope data were extracted from the 250 m digital elevation model (DEM) released by the Resource and Environment Data Center of the Chinese Academy of Sciences (https://www.resdc.cn/data.aspx?DATAID=123). Population density data were obtained from the LandScan Global High-Resolution Population Dataset (https://landscan.ornl.gov/). County-level per capita GDP data were sourced from the EPS Data Platform (https://www.epsnet.com.cn/).

2.3 Research Methods

2.3.1 VCS Estimation

NPP can be estimated based on the amount of carbon dioxide (CO_2) absorbed through plant photosynthesis and the content of dry matter produced [22, 23]. The chemical reaction process is as follows:

$$6CO_2 + 6H_2O \xrightarrow{\text{light, chloroplast, enzyme}} C_6H_{12}O_6 + 6O_2 \quad (1)$$

Based on the above reaction equation, plants consume 1.62 g of CO_2 to synthesize 1 g of dry matter through photosynthesis. Carbon content constitutes approximately 45% of the total NPP in dry matter. Therefore, the VCS can be calculated as follows:

$$\mathrm{VCS} = 1.62 \times (\mathrm{NPP}/0.45) \quad (2)$$

where VCS represents the VCS, expressed as carbon mass, with units of grams per square meter per year [g C m^{-2} a^{-1}]. NPP represents the net primary productivity of vegetation, similarly expressed as

carbon mass, with units of grams per square meter per year [g C m^{-2} a^{-1}].

2.3.2 Standard Deviation Ellipse(SDE) and Centroid Shift

SDE is a spatial statistical method used to characterize the distribution patterns and evolutionary processes of geographical elements. Key parameters of this method include the semi-major axis, semi-minor axis, and orientation, which respectively indicate the directional distribution and spatial extent of VCS [24]. The orientation represents the rotation angle of the semi-major axis measured clockwise from due north. This analytical model can be implemented using the Spatial Statistics Tools module in ArcGIS 10.7. The key parameters are calculated as follows:

The coordinates of the SDE centroid were computed as:

$$SDE_x = \sqrt{\sum_{n}^{i=1} \left(x_i - \overline{X}\right)^2 / n}$$
$$SDE_y = \sqrt{\sum_{n}^{i=1} \left(y_i - \overline{Y}\right)^2 / n} \quad (3)$$

where SDE_x and SDE_y denote the coordinates of the centroid of the SDE; (x_i,y_i) represents the spatial coordinates of the i-th geographic unit; i indicates the VCS quantity of the i-th unit (expressed in g C m^{-2} a^{-1}); $\bar{x}$, $\bar{y}$ is the mean center of the geographic units; n signifies the total number of geographic units.

The standard deviations for the semi-major and semi-minor axes of the SDE are calculated as follows:

$$\sigma_x = \sqrt{2}\sqrt{\frac{\sum_{i=1}^{n}\left(\overline{x}_i \cos\theta - \overline{y}_i \sin\theta\right)^2}{n}}$$
$$\sigma_y = \sqrt{2}\sqrt{\frac{\sum_{i=1}^{n}\left(\overline{x}_i \sin\theta - \overline{y}_i \cos\theta\right)^2}{n}} \quad (4)$$

where σ_x and σ_y represent the standard deviations along the X-axis and Y-axis, respectively.

The centroid coordinates of VCS are calculated using the following principal formula (5):

$$X = \frac{\sum_{i=1}^{n} N_i \times x_i}{\sum_{i=1}^{n} N_i}, Y = \frac{\sum_{i=1}^{n} N_i \times y_i}{\sum_{i=1}^{n} N_i} \quad (5)$$

where X and Y denote the coordinates of the VCS centroid; N_i represents the VCS quantity of the i-th geographic unit (in g C m^{-2} a^{-1}); (x_i, y_i) indicates the centroid coordinates of the i-th sub-administrative region; n is the total number of geographic units.

The spatial shift of the VCS centroid over time reflects the dynamics of spatial redistribution. Migration distance and direction were calculated to trace centroid movement trajectories [25]. The migration distance and directional angle are calculated as follows (Equation 6 and equation 7):

$$Dt = \sqrt{\left(x_{t1} - x_{t2}\right)^2 + \left(y_{t1} - y_{t2}\right)^2} \quad (6)$$

$$\theta t = t = arctan\frac{y_{t2} - y_{t1}}{x_{t2} - x_{t1}} \quad (7)$$

where x_{ti}, y_{ti} denotes the coordinates of the VCS centroid for year t_i.

2.3.3 Spatial Correlation Analysis

Global Spatial Autocorrelation In studying VCS within the CCEC, global spatial autocorrelation analysis is employed to assess the spatial distribution patterns of VCS [26]. This method quantifies the spatial dependence of VCS, revealing overall regional clustering or dispersion patterns. The Moran's I index is typically used for this purpose, calculated as follows:

$$I = \frac{\sum_i^n \sum_{j\neq 1}^n W_{ij}\left(x_i - \overline{x}\right)}{s^2 \sum_i^n \sum_{j\neq 1}^n w_{ij}} \quad (8)$$

where I denotes the global spatial autocorrelation index; S represents the standard deviation of VCS values; w_{ij} is the spatial weight matrix, reflecting the adjacency relationships between geographic units within the study area; n indicates the total number of geographic units; x_i and x_j represent the VCS quantities of units i and j, respectively (in g C m^{-2} a^{-1}); $\bar{x}$ is the mean x value across all units. The spatial weight $w_{ij} = 1$ indicates that region i and region j share a common boundary, signifying an adjacency relationship; otherwise, $w_{ij} = 0$. A positive value of Moran's I suggests that VCS exhibit a spatially clustered pattern; a negative value indicates a spatially dispersed pattern; and a value close to zero implies that the distribution of VCS is approximately random (not statistically significant).

Local Spatial Autocorrelation Local spatial autocorrelation analysis focuses on the distribution characteristics of attribute values across heterogeneous space. This method quantifies the local spatial association of VCS between each geographic unit and its neighboring areas. The Local Moran's I statistic is commonly employed, calculated as follows:

$$I_i = z_i \sum_{j \neq i}^{n} W_{ij} Z_j \tag{9}$$

where I_i represents the local spatial autocorrelation index for geographical unit i; z_i and z_j are the standardized values of VCS quantities for units i and j, respectively; w_{ij} denotes the spatial weight matrix. A positive I_i value indicates localized clustering of VCS, while a negative value signifies spatial dispersion.

2.3.4 Geodetector

Geodetector is a statistical method designed to identify spatial heterogeneity in geographical elements and reveal their driving factors. Its core principle involves partitioning the study area into subregions and assessing spatial heterogeneity by comparing the global variance to the sum of variances within subregions. This method quantifies the influence of both natural factors (rain, temperature, altitude, gradient) and anthropogenic factors (population density, per capita GDP) on the spatial differentiation of VCS [27]. We employ the determining power metric q to measure the impact of each factor on the spatiotemporal evolution of VCS eco-efficiency within the CCEC. The q statistic is calculated as follows:

$$q = 1 - \frac{1}{n\sigma^2} \sum_{h=1}^{m} n_h \cdot \sigma_h^2 \tag{10}$$

where the q-statistic ranges within [0,1], with higher values indicating stronger explanatory power of variable Z_i over the spatiotemporal evolution of VCS eco-efficiency. A value of $q = 0$ denotes that Z_i fails to explain the spatial distribution of VCS eco-efficiency, while $q = 1$ signifies that Z_i fully determines its spatial distribution. Here, $h = 1, 2, \ldots, m$ represents the strata partitioning for either independent variable Z or dependent variable Y; n denotes the total number of samples across the study area; σ^2 is the global variance; n_h indicates the sample count within stratum h; and σ_h^2 denotes the variance of dependent variable Y in stratum h.

The interaction detector assesses the strength and direction of bivariate interactions by comparing the q-values of individual variables with those after spatial overlay. It further evaluates whether such interactions alter the explanatory power of single variables regarding the spatial heterogeneity of the dependent variable. Specifically, this method compares the q-statistics of variables Z_i, Z_j, and their interaction term ($q(Z_i)$, $q(Z_j)$, $q(Z_i \cap Z_j)$) to determine interaction types: Nonlinear Weakening: When $q(Z_i \cap Z_j) < \min(q(Z_i), q(Z_j))$; Single-Factor Nonlinear Weakening: When $\min(q(Z_i), q(Z_j)) < q(Z_i \cap Z_j) < \max(q(Z_i), q(Z_j))$; Bilinear Enhancement: When $\max(q(Z_i), q(Z_j)) < q(Z_i \cap Z_j)$; Independence: When $q(Z_i \cap Z_j) = q(Z_i) + q(Z_j)$; Nonlinear Enhancement: When $q(Z_i \cap Z_j) > q(Z_i) + q(Z_j)$.

3 Research Results

3.1 Spatiotemporal Patterns

3.1.1 Temporal Dynamics

As shown in Figure 2, the VCS of the CCEC exhibited a long-term fluctuating upward trend between 2002 and 2022. In terms of temporal sequence, the early stage (2002–2011) was characterized by relatively low VCS levels with pronounced fluctuations; during the middle stage (2011–2015), VCS entered a period of rapid growth, with values rising steadily over time; and in the late stage (2015–2022), although interannual oscillations persisted, the overall level remained within a high-value range.

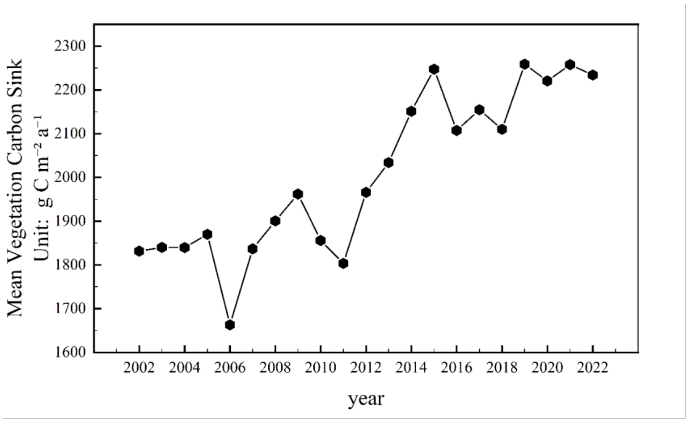

Figure 2. Temporal Variation of VCS in the CCEC.

The peak value occurred in 2019 (2258.90 g C m^{-2} a^{-1}), with secondary peaks in 2015 (2247.49 g C m^{-2} a^{-1}) and 2021 (2257.93 g C m^{-2} a^{-1}), forming a "clustered high-value peak." This pattern reflects the synergistic enhancement of biomass accumulation and vegetation community optimization—such as the succession

from coniferous to mixed forests—under the coupling of long-term ecological policy interventions (e.g., the CCEC Ecological Barrier Construction Project) and favorable climatic conditions (e.g., the strong East Asian Summer Monsoon in 2019 that brought abundant precipitation [28]). In contrast, VCS in 2006 experienced a sudden drop, falling by 207.00 g C m^{-2} a^{-1} (11.07%) compared with 2005 and remaining 173.89 g C m^{-2} a^{-1} lower than in 2007, representing an abrupt single-year trough. Historical climate records confirm that the CCEC suffered a once-in-a-century extreme heat and drought event in 2006 [29, 30], during which the mean temperature in Chongqing was 2.1°C above normal and precipitation was reduced by about 30%. Such extreme conditions suppressed photosynthesis, exacerbated evapotranspiration, and increased wildfire risks, collectively imposing a "cliff-edge shock" on the VCS system.

3.1.2 *Spatial Variation*

Based on ArcGIS 10.7, the spatial distribution of Vegetation Carbon Sinks (VCS) in the Chengdu-Chongqing Economic Circle (CCEC) at the county scale was obtained for 2002, 2007, 2012, 2017, and 2022 (as shown in Figure 3). The results show that the high-value areas of VCS exhibited a distinct "three-belt agglomeration" pattern, with persistent clustering in the Southwestern Sichuan Mountains, the Southeastern Chongqing Mountains, the Southeastern Sichuan Mountains, and the mountainous areas surrounding the Sichuan Basin. Among these, the Southwestern Sichuan Mountains belong to the eastern margin of the Hengduan Mountain system, the Southeastern Chongqing Mountains form part of the Wuling Mountain region in southeastern Chongqing, while the Southeastern Sichuan Mountains and the peripheral ranges of the Sichuan Basin are situated along the basin's margins. These regions are predominantly characterized by mountainous and hilly landforms, high natural vegetation cover, and strong ecosystem integrity, all of which contribute to their outstanding baseline carbon sink capacity [31]. By contrast, low-value areas were consistently concentrated in two main types of regions. The first comprises plains and shallow hills within the Sichuan Basin, most notably the core area of the Chengdu Plain and the western valley zone of Chongqing, where rapid urbanization and extensive agricultural development have encroached upon natural ecosystems. Vegetation in these areas is dominated by plantations and croplands, resulting in a low baseline for carbon sequestration [32]. The second type includes the relatively gentle terrain in northeastern Sichuan, such as parts of Nanchong

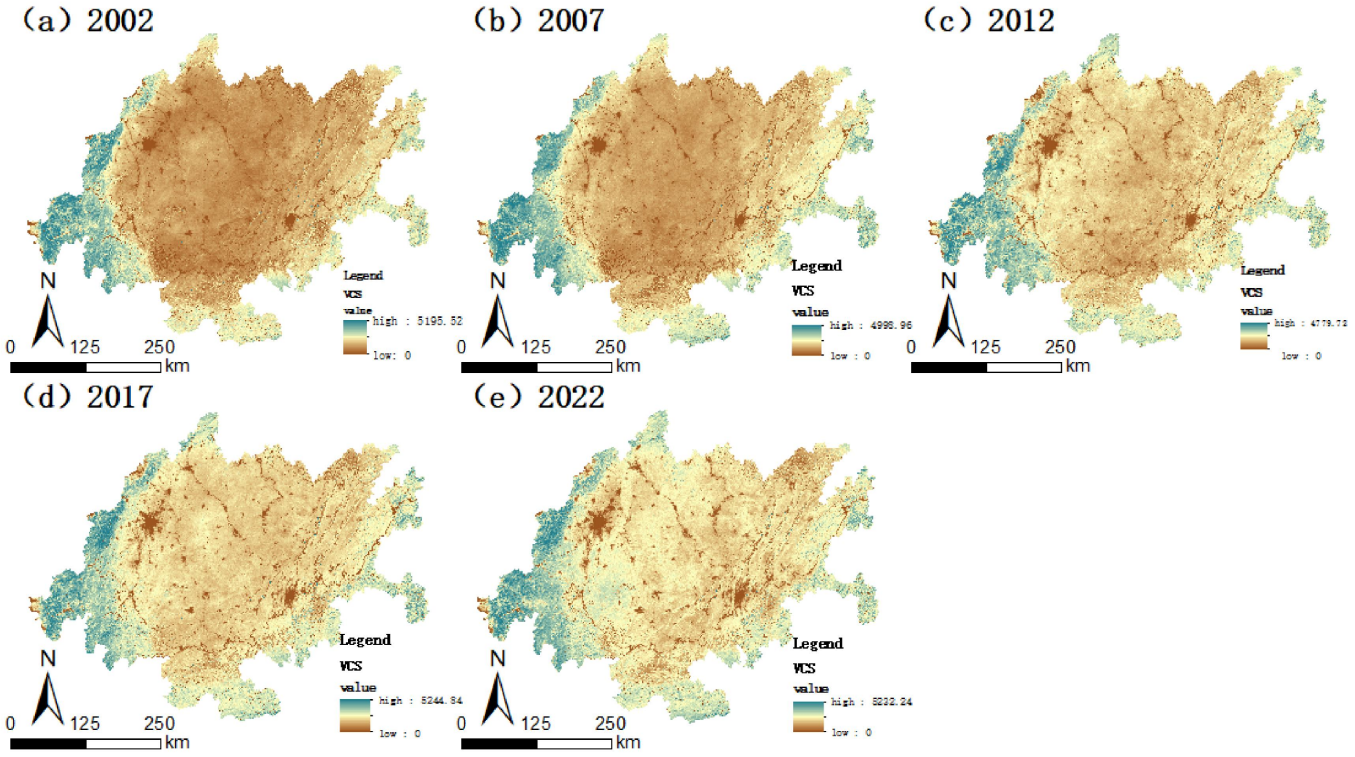

Figure 3. Spatial variation of VCS in the CCEC.

Table 1. Results of SDE and Centroid Shift.

Year	Semi-major axis (km)	Semi-minor axis (km)	Center X/°	Center Y/°	Azimuth (°)
2002	235.217	150.862	105.371	29.967	75.456
2007	236.983	151.908	105.413	29.977	75.596
2012	229.086	150.149	105.407	29.999	73.826
2017	226.569	151.037	105.410	29.998	74.632
2022	224.616	150.545	105.390	30.000	74.181

and Dazhou, where a long history of agricultural exploitation has left little natural vegetation and thus weakened carbon sink capacity.

3.1.3 SDE and Centroid Shift

Based on ArcGIS 10.7, a SDE and centroid shift analysis of VCS in the CCEC was conducted (Table 1 and Figure 4). Overall, from 2002 to 2022, the SDE of VCS consistently maintained a northeast–southwest orientation, with azimuth values falling within the range of 73°–76°.

During this period, the centroid coordinates of VCS ranged between 105.371°E–105.413°E and 29.967°N–30.000°N, with the centroid consistently located in Anyue County, Sichuan Province. This area lies within the hilly transitional zone in the central part of the CCEC, corresponding to the topographic gradient from the northeastern Sichuan Basin to the southwestern mountainous areas, and aligning with the baseline spatial framework of low VCS values in the basin and high VCS values in the mountains. As shown in Figure 4(c), the centroid migration trajectory followed a fluctuating but convergent path—moving northeast → northwest → southeast → northwest—and in the long term, shifted slightly toward the interior of the Sichuan Basin. This indicates an "inward convergence and reshaping" effect of increasing VCS within the basin on the overall spatial pattern [33].

The semi-major axis contracted steadily from 235.217 km in 2002 to 224.616 km in 2022, while the semi-minor axis decreased slightly from 150.862 km to 150.545 km, suggesting a continuous reduction in spatial dispersion and a tendency toward centripetal agglomeration. Meanwhile, the azimuth rotated from 75.456° in 2002 to 74.181° in 2022, reflecting asymmetric growth between the Southwestern Sichuan Mountains (the southwestern end of the high-value zone) and the Southeastern Chongqing Mountains (the southeastern end of the high-value zone). In the Southwestern Sichuan region, dominated by primary forests, VCS growth relied primarily

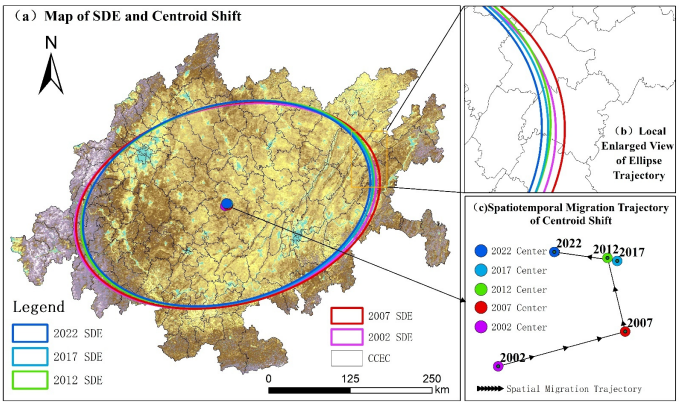

Figure 4. Standard Deviational Ellipse and centroid shift of VCS in the CCEC.

on natural succession, resulting in relatively slow increases but sustained high levels. By contrast, in the Southeastern Chongqing region, policy measures designating the area as an "Ecological Protection and Development Zone" accelerated the efficiency gains of plantation forests, leading the ellipse's major axis to first adjust slightly southeastward. Later, with reinforced ecological protection in the Southwestern Sichuan region, such as the implementation of natural forest conservation in Liangshan Prefecture, the ellipse stabilized again.

3.1.4 Spatial Correlation Analysis

Global Spatial Autocorrelation To further examine the spatial association and evolutionary characteristics of VCS in the CCEC, we employed the Global Moran's I index. The results are presented in Table 2. It can be observed that the Global Moran's I of VCS in the CCEC exhibited a fluctuating trend of "initial increase, subsequent decline, and then a slight rebound." With z-scores ranging between 121.35 and 97.72 and p-values consistently equal to 0.00, the null hypothesis of "spatial randomness" can be rejected at the 1% significance level for all years, indicating that VCS in the CCEC displayed significant positive spatial autocorrelation at the grid scale. Since global spatial autocorrelation cannot

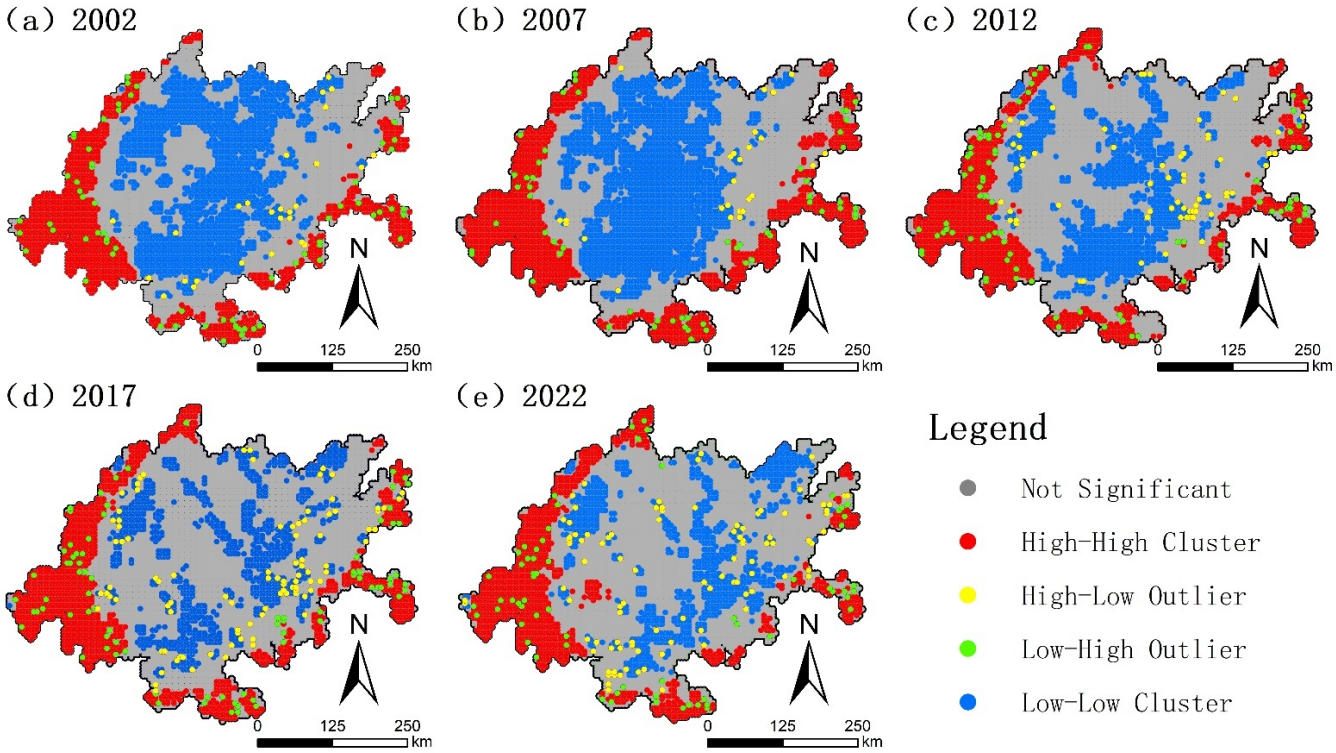

Figure 5. Local Moran's I of VCS in the CCEC.

capture regional heterogeneity, we further applied local spatial autocorrelation analysis to investigate localized variations in VCS across the CCEC.

Table 2. Global Moran's I Index of VCS in the CCEC.

Year	Moran's *I*	Z-score (standard deviation)	p-value
2002	0.730765	121.354154	0.00
2007	0.76415	126.806458	0.00
2012	0.615729	102.191398	0.00
2017	0.588778	97.724444	0.00
2022	0.601567	99.915879	0.00

Local Spatial Autocorrelation To reveal the local spatial characteristics of VCS at the county scale, we calculated the Local Moran's I index for the years 2002, 2007, 2012, 2017, and 2022 using ArcGIS 10.7 (as shown in Figure 5). In the maps, red (HH) represents "high-value VCS grids adjacent to other high-value VCS grids," blue (LL) represents "low-value VCS grids adjacent to other low-value VCS grids," yellow (HL) denotes "high-value VCS grids surrounded by low-value VCS grids," green (LH) denotes "low-value VCS grids surrounded by high-value VCS grids," while gray areas indicate statistically insignificant spatial associations.

From the perspective of spatial distribution, the local spatial association of VCS in the CCEC was overwhelmingly dominated by positive correlations (HH and LL), while negative correlations (HL and LH) accounted for a small proportion and were scattered. HH clusters were persistently concentrated in the Southeastern Chongqing Mountains (e.g., the Qianjiang–Xiushan area), the Southeastern Sichuan Mountains (e.g., the Yibin–Luzhou region), and the Southwestern Sichuan Mountains (e.g., Liangshan Prefecture). LL clusters were consistently concentrated within the plains and shallow hills of the Sichuan Basin interior, particularly in the core of the Chengdu Plain and the western valley zone of Chongqing. HL and LH outliers were sporadically distributed in transitional zones between mountainous and basin areas, such as the peripheral mountain edges of the basin and the hilly–mountainous junctions of northeastern Sichuan. In terms of temporal dynamics, the number of HH clusters increased steadily, LL clusters first expanded and then contracted, while HL and LH clusters declined initially and subsequently stabilized.

3.2 Driving Factors analysis

3.2.1 Single-Factor Detection

Based on the spatial differentiation characteristics of the topography–climate framework and human activity intensity in the CCEC, six driving factors were selected. These factors were categorized

into two dimensions: natural background variables (rain, temperature, gradient, and altitude) and anthropogenic interventions (population density and per capita GDP). Five temporal cross-sections (2002, 2007, 2012, 2017, and 2022) were chosen, and the Geodetector was applied to assess the explanatory power of each driving factor on the spatial differentiation of VCS in the CCEC, as well as to explore the interaction mechanisms among these factors.

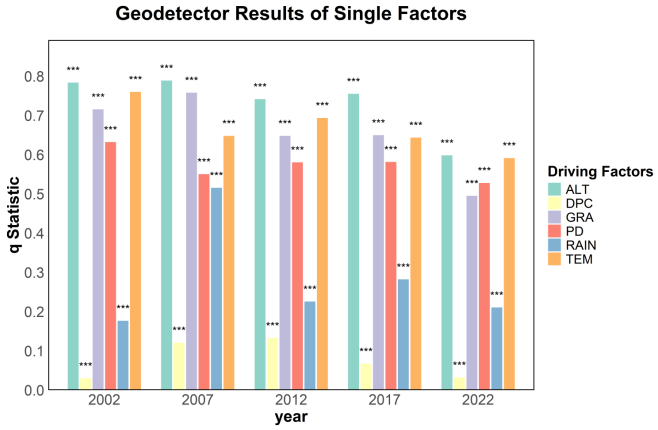

Figure 6. Single-factor detection of VCS in the CCEC.

According to the single-factor detection results (as shown in Figure 6), the p-values of all factors were 0.000 during the study period, passing the 1% significance test. This indicates that rain (RAIN), temperature (TEM), gradient (GRA), altitude (ALT), population density (PD), and per capita GDP (DPC) consistently exerted significant influences on VCS levels and demonstrated strong explanatory power for their spatial differentiation. More specifically, natural factors as a whole had stronger explanatory power (q-values) for VCS differentiation than anthropogenic factors [34]. Among them, ALT was the dominant and core factor, with mean q-values consistently exceeding 0.76. High-elevation regions such as the Southwestern Sichuan Mountains and the Southeastern Chongqing Mountains are characterized by extensive primary forest cover and strong carbon sink capacity, whereas the low-elevation Sichuan Basin has experienced urbanization and agricultural expansion, leading to fragmented vegetation and weak baseline carbon sinks. Altitude, therefore, directly shapes the spatial framework of "mountainous high VCS–basin low VCS" through its vertical topographic gradient. TEM ($q = 0.59$–0.76) further reinforced this differentiation by regulating the length of the growing season and photosynthetic efficiency, resulting in higher VCS in mountainous areas (longer growing seasons, stronger carbon sequestration) and lower VCS in the basin (shorter growing seasons, dominance of artificial vegetation). GRA ($q = 0.49$–0.76) intensified differentiation by reflecting the spatial dichotomy between steep zones under ecological protection (e.g., reforestation programs) and flat zones under intensive human development (e.g., urban expansion). RAIN ($q = 0.17$–0.28) exerted the weakest explanatory effect, consistent with the generally favorable hydrothermal balance across the region.

Among anthropogenic factors, PD ($q = 0.52$–0.63) captured the phased dynamics of human–land interactions, reflecting the early stage of ecological space encroachment by urbanization followed by a later stage of ecological restoration projects that enhanced carbon sink capacity. By contrast, DPC ($q = 0.03$–0.13) demonstrated relatively limited explanatory power, indicating that the feedback mechanism of ecological product value realization is still underdeveloped and its role in driving VCS differentiation remains weak.

3.2.2 *Interaction Detection*

The interaction detection results show that combinations of multiple driving factors had stronger explanatory power for the spatial differentiation of VCS than single factors [35]. Based on the Geodetector interaction results (as shown in Figure 7), the multi-factor synergistic effects underlying VCS spatial heterogeneity in the CCEC can be further elucidated. In terms of interaction types, the interactions among driving factors across all years were overwhelmingly dominated by "bi-factor enhancement" and "nonlinear enhancement," with no evidence of "linear weakening" or "nonlinear weakening." This indicates that both natural background and anthropogenic intervention factors exerted a "synergistic amplification" effect on VCS differentiation, whereby the explanatory power of individual factors was significantly strengthened through their interactions.

Regarding different interaction combinations and mechanisms, natural–natural factor interactions (e.g., TEM with RAIN, GRA with ALT) formed the core driving cluster. In 2002, the q-value for TEM∩RAIN reached 0.93, reflecting the coupled regulation of vegetation carbon sequestration by hydrothermal conditions-temperature determining the length of the growing season and precipitation ensuring water availability. This amplified the contrast between mountainous high-altitude zones with favorable hydrothermal balance and strong forest carbon

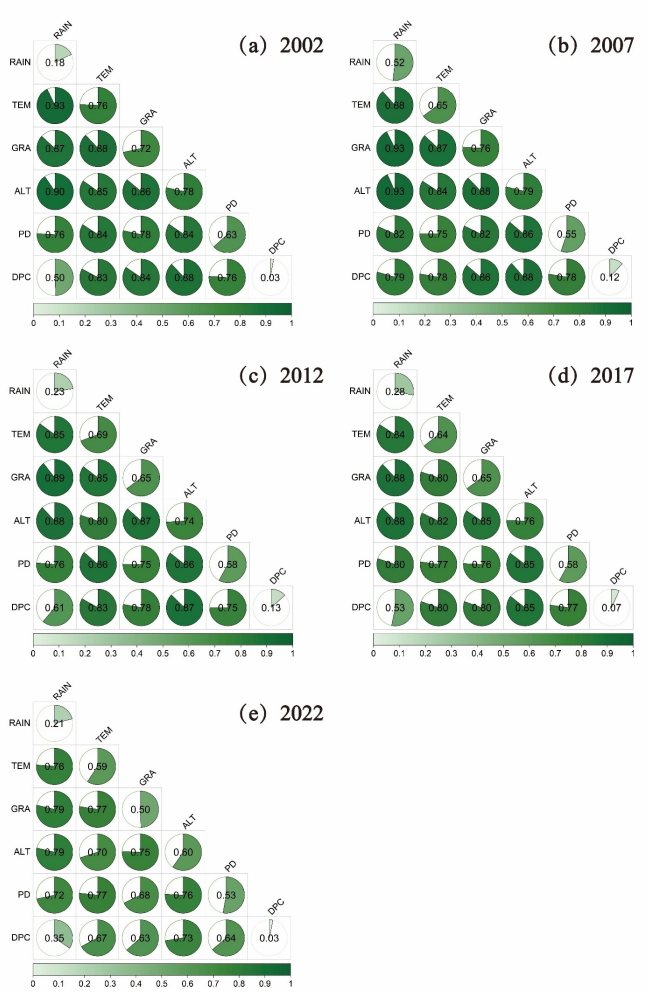

Figure 7. Heatmap of interactive factor detection of VCS in the CCEC.

sinks, and basin low-altitude zones with mismatched conditions and constrained carbon sinks. In 2007, the q-value for GRA∩RAIN also reached 0.93, highlighting how the coupling of slope (affecting soil erosion risk) and precipitation (influencing runoff intensity) reinforced the spatial dichotomy between steep-slope ecological conservation areas (high VCS) and gently sloping zones under human exploitation (low VCS).

Interactions between natural and anthropogenic factors (e.g., ALT with PD, TEM with DPC) revealed stage-specific "human–environment interaction" characteristics. After 2012, the q-value for ALT∩PD stabilized above 0.75, indicating a synergistic effect in which high-altitude mountains (where ALT constrained development intensity) were preserved through ecological protection, while densely populated low-altitude basins (with high PD) underwent ecological restoration projects such as urban greening. This reinforced the spatial contrast of "mountain carbon sequestration–basin carbon enhancement" as human–environment interactions intensified. The q-value for DPC∩TEM increased to 0.57 by 2022, suggesting that economic development began to exert a "counter-regulatory" effect on temperature-driven differentiation of carbon sinks through measures such as temperature-controlled agricultural facilities and urban green space cooling. Although weaker than natural–natural interactions, this reflects a potential pathway for realizing the value of ecological products.

From a temporal perspective, during 2002–2007, natural–natural interactions consistently exhibited higher q-values than natural–human interactions, confirming that topography and climate formed the fundamental baseline for VCS differentiation. Between 2012 and 2022, however, the q-values of natural–human interactions increased steadily (e.g., PD∩ALT remaining above 0.75; DPC∩TEM rising from 0.50 to 0.57), reflecting the shift under CCEC's eco-cooperation policies from passive human adaptation to active regulation of natural systems. The synergistic effects of ecological restoration and economic development thus became increasingly prominent.

In summary, the spatial differentiation of VCS in the CCEC is the outcome of a coupled natural–human system rather than the effect of a single factor. Natural factors remain the dominant drivers, with elevation and temperature exerting the strongest influences, while the explanatory power of multiple-factor interactions surpasses that of individual factors. This further demonstrates that changes in the spatial pattern of VCS are primarily shaped by natural conditions but are jointly reinforced by multiple interacting drivers.

4 Discussion

This study examined the spatiotemporal evolution of VCS and their driving mechanisms in the CCEC from 2002 to 2022 at the county scale. Compared with conventional grid-based studies, county-level analysis aligns more closely with the administrative boundaries that frame ecological governance, thereby bridging the gap between macro-level spatial patterns and micro-level policy implementation. This perspective offers new insights for improving the spatial targeting of ecological policies. By systematically analyzing the shifts in VCS centroids, spatial clustering dynamics, and changes in Standard Deviational Ellipses, the results show that VCS exhibited an overall upward but fluctuating trend between 2002 and 2022, with an

anomalously low value in 2006. The sharp decline in that year was attributable to extreme heat events in Sichuan and Chongqing, which significantly reduced vegetation carbon sequestration [36]. Spatially, VCS displayed a "high on the western, southern, and eastern margins, low in the middle" distribution pattern. This differs in certain respects from previous studies on different geomorphic units [37, 38], though most studies consistently report a gradual decline in VCS from mountainous high-value areas toward the basin low-value zones. The present findings further suggest that, under ecological engineering policies, restoration effects in low-VCS regions are beginning to emerge [39, 40]. Meanwhile, the VCS centroid remained located near Anyue County in Sichuan throughout the 20-year period, indicating that although increases in carbon sinks diffused outward, the core contribution areas were still strongly constrained by topography and natural background conditions. This underscores the foundational role of mountainous regions in shaping regional carbon sink patterns [41, 42].

Compared with grid-scale analyses, county-level investigation not only better reflects the realities of policy management but also enhances the understanding of how ecological policies interact with spatial responses within administrative units. The results indicate pronounced heterogeneity in carbon sink capacity across counties, with spatial differentiation exhibiting persistent evolutionary features. For instance, some plateau and mountainous counties maintained consistently high carbon sink capacities over the long term [43, 44], while plain counties with high levels of urbanization exhibited a fluctuating trajectory of initial suppression followed by recovery [45, 46]. Such spatial heterogeneity is difficult to detect using grid-based units and even harder to translate into differentiated policy responses. Consequently, spatiotemporal pattern recognition at the county scale is essential for revealing the alignment between policy interventions and geographic contexts, thereby enhancing the precision of carbon sink management.

In terms of driving mechanisms, the Geodetector model demonstrated stronger spatial adaptability and explanatory capacity than traditional linear approaches. This study found that natural factors such as elevation and slope consistently exhibited strong explanatory power for VCS patterns, with elevation remaining the dominant factor ($q > 0.76$). This reflects the strong constraint of natural background conditions on vegetation growth and carbon sequestration potential [47, 48], while also showing both similarities and differences with dominant drivers reported in other study areas [49]. Furthermore, the interaction detection results revealed widespread "nonlinear enhancement" or "bi-factor enhancement" effects between natural and anthropogenic factors, such as temperature with per capita GDP and elevation with population density. This indicates that regional VCS patterns are not shaped by single factors but rather emerge from the compounded effects of human activities superimposed on natural baselines [50]. The findings also highlight the necessity of employing the Geodetector: on one hand, it avoids biases introduced by linear assumptions; on the other, by identifying interaction mechanisms, it helps uncover the true logic of carbon sink distribution under the coupled dynamics of the human–environment system [51].

In conclusion, by integrating county-scale empirical analysis with the Geodetector approach, this study not only deepens the understanding of the spatiotemporal dynamics of VCS in the CCEC but also expands the methodological paradigm for investigating carbon sink drivers. These findings provide practical references for regional ecological governance, precision-based carbon sink enhancement, and the design of "differentiated dual-carbon pathways." Nonetheless, limitations remain: the analysis was constrained by data availability, preventing the inclusion of certain socioeconomic variables; and while the Geodetector effectively identifies mechanisms of spatial differentiation, it cannot reveal causal relationships between variables. Future studies could incorporate panel econometric models or causal inference approaches, alongside high-resolution land use and ecological policy datasets, to further advance the dynamic identification of carbon sink evolution mechanisms and their policy feedback processes.

5 Conclusion

(1) From 2002 to 2022, county-level VCS in the CCEC exhibited a fluctuating but overall increasing trend. The centroid of VCS remained stably located near Anyue County in the central Sichuan hilly region, while the spatial distribution revealed a structural pattern of "mountainous high-value clusters and plain low-value diffusion." The Standard Deviational Ellipse indicated that the spatial dispersion of VCS gradually converged, showing an overall tendency toward centripetal agglomeration. Meanwhile, spatial autocorrelation analysis confirmed significant

clustering of VCS distribution, with local spatial structures evolving from "strong aggregation" toward "weaker convergence."

(2) The driving mechanisms of VCS identified at the county scale demonstrated that natural factors remain the dominant forces, with elevation, temperature, and slope exerting particularly strong explanatory power in shaping spatial differentiation. These factors collectively established a spatial framework dominated by the mountain–plain gradient. In addition, the Geodetector identified widespread "nonlinear enhancement" interactions between natural and anthropogenic factors. Notably, combinations such as "ALT∩PD" and "TEM∩DPC" amplified the heterogeneity of VCS spatial patterns, underscoring the complex driving characteristics of human–environment coupling.

(3) By integrating county-level perspectives with the Geodetector model, this study provides an innovative approach for identifying both the spatial patterns and underlying mechanisms of VCS from an "administrative unit perspective." This integration offers new empirical support for regionally differentiated ecological governance and the implementation of dual-carbon strategies. Nevertheless, limitations remain, including the omission of certain socioeconomic variables and the inability to explicitly identify causal relationships. Future research should incorporate multi-source remote sensing data and policy databases to expand the dimensionality of driving factors and explanatory mechanisms, thereby enhancing the dynamic understanding of carbon sink evolution and strengthening policy responsiveness.

Data Availability Statement

Data will be made available on request.

Funding

This work was supported by the National Undergraduate Innovation Training Program under Grant 202510622017, and the Sichuan Provincial Undergraduate Innovation Training Program under Grant S202410622069 and Grant S202510622068.

Conflicts of Interest

The authors declare no conflicts of interest.

Ethical Approval and Consent to Participate

Not applicable.

References

[1] Soininen, N., Ruhl, J. B., Cosens, B., & Gunderson, L. (2025). Governing complexity: A comparative assessment of four governance models with applications to climate change mitigation and adaptation. *Environmental Innovation and Societal Transitions, 57*, 101020. [Crossref]

[2] Fan, Y., & Wei, F. (2022). Contributions of natural carbon sink capacity and carbon neutrality in the context of net-zero carbon cities: A case study of Hangzhou. *Sustainability, 14*(5), 2680. [Crossref]

[3] Ge, W., Deng, L., Wang, F., & Han, J. (2021). Quantifying the contributions of human activities and climate change to vegetation net primary productivity dynamics in China from 2001 to 2016. *Science of the Total Environment, 773*, 145648. [Crossref]

[4] Liu, X., Wang, P., Song, H., & Zeng, X. (2021). Determinants of net primary productivity: Low-carbon development from the perspective of carbon sequestration. *Technological Forecasting and Social Change, 172*, 121006. [Crossref]

[5] Shi, S., Zhu, L., Luo, Z., & Qiu, H. (2023). Quantitative analysis of the contributions of climatic and anthropogenic factors to the variation in net primary productivity, China. *Remote Sensing, 15*(3), 789. [Crossref]

[6] Wang, T., Gao, M., Fu, Q., & Chen, J. (2024). Spatiotemporal dynamics and influencing factors of vegetation net primary productivity in the Yangtze River Delta Region, China. *Land, 13*(4), 440. [Crossref]

[7] Lu, Z., Chen, P., Yang, Y., Zhang, S., Zhang, C., & Zhu, H. (2023). Exploring quantification and analyzing driving force for spatial and temporal differentiation characteristics of vegetation net primary productivity in Shandong Province, China. *Ecological Indicators, 153*, 110471. [Crossref]

[8] Bogale, T., Degefa, S., Dalle, G., & Abebe, G. (2024). Spatiotemporal dynamics of vegetation net primary productivity and its response to climate variability. *Environmental Systems Research, 13*(1), 47. [Crossref]

[9] Yu-hang, H. A. N., & Zhen, H. A. N. (2025). Spatial and Temporal Variation of Vegetation Carbon Source/Sink in Coastal City and Its Effecting Factors. *Chinese Journal of Agrometeorology, 46*(4), 435.

[10] Song, S., Kong, M., Su, M., & Ma, Y. (2024). Study on carbon sink of cropland and influencing factors: A multiscale analysis based on geographical weighted regression model. *Journal of Cleaner Production, 447*, 141455. [Crossref]

[11] Zhang, X., Wang, Y. P., Peng, S., Rayner, P. J., Ciais, P., Silver, J. D., ... & Zheng, X. (2018). Dominant regions

and drivers of the variability of the global land carbon sink across timescales. *Global Change Biology, 24*(9), 3954-3968. [Crossref]

[12] Li, C., & Zhang, S. (2024). Assessing and explaining rising global carbon sink capacity in karst ecosystems. *Journal of Cleaner Production, 477*, 143862. [Crossref]

[13] Bao, G., Bao, Y., Qin, Z., Xin, X., Bao, Y., Bayarsaikan, S., ... & Chuntai, B. (2016). Modeling net primary productivity of terrestrial ecosystems in the semi-arid climate of the Mongolian Plateau using LSWI-based CASA ecosystem model. *International Journal of Applied Earth Observation and Geoinformation, 46*, 84-93. [Crossref]

[14] Bulkeley, H. (2005). Reconfiguring environmental governance: Towards a politics of scales and networks. *Political geography, 24*(8), 875-902. [Crossref]

[15] Wang, J. F., & Xu, C. D. (2017). Geodetector: Principle and prospective. *Acta geographica sinica, 72*(1), 116-134.

[16] Li, F., Nan, T., Zhang, H., Luo, K., Xiang, K., & Peng, Y. (2025). Evaluating Ecological Vulnerability and Its Driving Mechanisms in the Dongting Lake Region from a Multi-Method Integrated Perspective: Based on Geodetector and Explainable Machine Learning. *Land, 14*(7), 1435.[Crossref]

[17] Wu, Q., & Dai, Y. (2024). Ecological Security Patterns Research Based on Ecosystem Services and Circuit Theory in Southwest China. *Sustainability, 16*(7), 2835. [Crossref]

[18] Zhang, X., Luo, H., Zeng, X., Zhou, C., Shu, Z., Li, H., ... & Liu, G. (2024). Research on regional economic development and natural disaster risk assessment under the goal of carbon peak and carbon neutrality: A case study in Chengdu-Chongqing economic circle. *Land Use Policy, 143*, 107206. [Crossref]

[19] Huang, H., & Yang, X. (2025). Spatiotemporal Evolution Mechanism and Dynamic Simulation of the Urban Resilience System in the Chengdu–Chongqing Economic Circle. *Sustainability (2071-1050), 17*(8). [Crossref]

[20] Xu, C., An, Q., Guo, Z., Yu, X., Zhang, J., & Tang, K. (2023). Comparative Study on Socio-Spatial Structures of the Typical Plain Cities of Chengdu and Beijing in Transitional China. *Sustainability, 15*(5), 4364. [Crossref]

[21] Darwent, D. F. (1969). Growth poles and growth centers in regional planning—a review. *Environment and Planning A, 1*(1), 5-31. [Crossref]

[22] Cleveland, C. C., Taylor, P., Chadwick, K. D., Dahlin, K., Doughty, C. E., Malhi, Y., ... & Townsend, A. R. (2015). A comparison of plot-based satellite and Earth system model estimates of tropical forest net primary production. *Global Biogeochemical Cycles, 29*(5), 626-644.[Crossref]

[23] Wang, C., Wang, L., Zhao, W., Zhang, Y., & Liu, Y. (2024). Analysis of Spatiotemporal Change and driving factors of NPP in Qilian Mountains from 2000 to 2020. *Rangeland Ecology & Management, 96*, 56-66. [Crossref]

[24] Hongzhang, C. H. E. N., Bing, Z. E. N. G., & Hong, G. U. O. (2022). Spatial-temporal pattern evolution and driving factors of county economy in the yellow river basin: based on the analysis of night light data. *Economic geography, 42*(11), 37-44. [Crossref]

[25] Feng, S., Hughes, A. C., Yang, Q., Li, L., & Li, C. (2025). Centroid-AME: An open-source software for estimating avian migration trajectories using population centroids movement in the annual cycle. *Ecological Informatics, 85*, 102983. [Crossref]

[26] Zhang, J., Shi, J., Wang, Y., & ZHAO, J. (2016). Spatial characteristics and dynamic change of innovation outputs in the Yangtze River Economic Belt [J]. *Progress in Geography, 35*(9), 1119-1128.

[27] Chen, M. H., Yue, H. J., Hao, Y. F., & Liu, W. F. (2021). The spatial disparity, dynamic evolution and driving factors of ecological efficiency in the Yellow River Basin. *J. Quant. Tech. Econ, 38*, 25-44.

[28] Liu, Y., Yan, M., Liu, J., Wang, S., Liu, Z., Ning, L., & Wang, Z. (2025). The co-evolution of East Asian subtropical westerly jet and East Asian summer monsoon during different time periods in the Holocene and its influence on precipitation patterns in China. *Science China Earth Sciences*, 1-16. [Crossref]

[29] Peng, J. B., Zhang, Q. Y., & Bueh, C. (2007). On the characteristics and possible causes of a severe drought and heat wave in the Sichuan-Chongqing region in 2006. *Climatic and Environmental research, 12*(3), 464-474.

[30] Wu, J., Gao, X. J., Zhang, D. F., Shi, Y., & Filippo, G. (2011). Regional climate model simulation of the climate effects of the Three Gorge Reservoir with specific application to the summer 2006 drought over the Sichuang-Chongqing area. *J Trop Meteorol, 27*(1), 44-52.

[31] Gogoi, A., Ahirwal, J., & Sahoo, U. K. (2022). Evaluation of ecosystem carbon storage in major forest types of Eastern Himalaya: Implications for carbon sink management. *Journal of Environmental Management, 302*, 113972. [Crossref]

[32] Padarian, J., Minasny, B., McBratney, A., & Smith, P. (2022). Soil carbon sequestration potential in global croplands. *PeerJ, 10*, e13740. [Crossref]

[33] Li, J. B., Zhang, C. L., Chen, H. M., Zhao, X. F., Li, Y., & Wang, P. Z. (2025). Spatio-temporal Characteristics and Influencing Factors of Carbon Sinks at the County Level in the Yancheng City. *Huan jing ke xue= Huanjing kexue, 46*(4), 1985-1994. [Crossref]

[34] Zhang, X., Zheng, Z., Sun, S., Wen, Y., & Chen, H. (2023). Study on the driving factors of ecosystem service value under the dual influence of natural environment and human activities. *Journal of Cleaner Production, 420*, 138408. [Crossref]

[35] Ding, X., Shu, Y., Tang, X., & Ma, J. (2022). Identifying

driving factors of basin ecosystem service value based on local bivariate spatial correlation patterns. *Land, 11*(10), 1852. [Crossref]

[36] Feng, H., Kang, P., Deng, Z., Zhao, W., Hua, M., Zhu, X., & Wang, Z. (2023). The impact of climate change and human activities to vegetation carbon sequestration variation in Sichuan and Chongqing. *Environmental Research, 238*, 117138. [Crossref]

[37] Harris, P. T., & Whiteway, T. (2011). Global distribution of large submarine canyons: Geomorphic differences between active and passive continental margins. *Marine Geology, 285*(1-4), 69-86.[Crossref]

[38] Xuan, Z. H. A. O., Xiangyang, Z. H. A. N. G., Guofa, L. I. U., & Tenglong, W. A. N. G. (2024). Research on the spatio-temporal variation of vegetation carbon sink and its correlation with climate in the Qinling Mountains of Shaanxi. *Bulletin of Surveying and Mapping*, (9), 55.

[39] Ye, M., Liao, L., Fu, T., & Lan, S. (2024). Do establishment of protected areas and implementation of regional policies both promote the forest NPP? Evidence from Wuyi Mountain in China based on PSM-DID. *Global Ecology and Conservation, 55*, e03210. [Crossref]

[40] Zhang, J., Wang, J., Chen, Y., Huang, S., & Liang, B. (2024). Spatiotemporal variation and prediction of NPP in Beijing-Tianjin-Hebei region by coupling PLUS and CASA models. *Ecological Informatics, 81*, 102620. [Crossref]

[41] Qing-Ling, S., Xian-Feng, F., Yong, G., & Bao-Lin, L. (2015). Topographical effects of climate data and their impacts on the estimation of net primary productivity in complex terrain: A case study in Wuling mountainous area, China. *Ecological informatics, 27*, 44-54. [Crossref]

[42] Chen, S., Ma, M., Wu, S., Tang, Q., & Wen, Z. (2023). Topography intensifies variations in the effect of human activities on forest NPP across altitude and slope gradients. *Environmental Development, 45*, 100826. [Crossref]

[43] Liu, J., Ji, Y. H., Zhou, G. S., Zhou, L., Lyu, X. M., & Zhou, M. Z. (2022). Temporal and spatial variations of net primary productivity (NPP) and its climate driving effect in the Qinghai-Tibet Plateau, China from 2000 to 2020. *Ying yong sheng tai xue bao= The Journal of Applied Ecology, 33*(6), 1533-1538. [Crossref]

[44] Long, B., Zeng, C., Zhou, T., Yang, Z., Rao, F., Li, J., ... & Tang, X. (2024). Quantifying the relative importance of influencing factors on NPP in Hengduan Mountains of the Tibetan Plateau from 2002 to 2021: A Dominance Analysis. *Ecological Informatics, 81*, 102636. [Crossref]

[45] Guo, L., Liu, R., Shoaib, M., Men, C., Wang, Q., Miao, Y., ... & Zhang, Y. (2021). Impacts of landscape change on net primary productivity by integrating remote sensing data and ecosystem model in a rapidly urbanizing region in China. *Journal of Cleaner Production, 325*, 129314. [Crossref]

[46] Hong, W., Ren, Z., Guo, Y., Wang, C., Cao, F., Zhang, P., ... & Ma, Z. (2024). Spatiotemporal changes in urban forest carbon sequestration capacity and its potential drivers in an urban agglomeration: Implications for urban CO2 emission mitigation under China's rapid urbanization. *Ecological Indicators, 159*, 111601. [Crossref]

[47] Sun, H., Chen, Y., Xiong, J., Ye, C., Yong, Z., Wang, Y., ... & Xu, S. (2022). Relationships between climate change, phenology, edaphic factors, and net primary productivity across the Tibetan Plateau. *International Journal of Applied Earth Observation and Geoinformation, 107*, 102708. [Crossref]

[48] Wang, Z., Dong, C., Dai, L., Wang, R., Liang, Q., He, L., & Wei, D. (2023). Spatiotemporal evolution and attribution analysis of grassland NPP in the Yellow River source region, China. *Ecological Informatics, 76*, 102135. [Crossref]

[49] Liang, W., Yang, Y., Fan, D., Guan, H., Zhang, T., Long, D., ... & Bai, D. (2015). Analysis of spatial and temporal patterns of net primary production and their climate controls in China from 1982 to 2010. *Agricultural and Forest Meteorology, 204*, 22-36. [Crossref]

[50] WANG, T. F., GONG, Z. W., & DENG, Y. J. (2022). Identification of priority areas for improving quality and efficiency of vegetation carbon sinks in Shaanxi province based on land use change. *Journal of Natural Resources, 37*(5), 1214-1232. [Crossref]

[51] Yao, N., Liu, G. Q., Yao, S. B., Deng, Y., Hou, M., & Zhang, X. (2022). Evaluating on effect of conversion from farmland to forest and grassland porject on ecosystem carbon storage in Loess Hilly-gully Region based on InVEST model. *Bulletin of Soil and Water Conservation, 42*(5), 329-336.

Wenjing Wang Pursuing a Bachelor's degree at Sichuan University of Science & Engineering. (Email: 23301030227@stu.suse.edu.cn)

Yuanjie Deng received his Ph.D. in Management from Northwest A&F University in 2022. His research focuses on resource economics and environmental management, with particular interests in ecological and environmental policy evaluation, the realization of ecological product value, land resource management, and GIS-based spatial analysis. (Email: ecodyj@suse.edu.cn)

Hua'e Dang Pursuing a Master's degree at Sichuan University of Science & Engineering. (Email: 324095114104@stu.suse.edu.cn)

Jincan Chen Pursuing a Bachelor's degree at Sichuan University of Science & Engineering. (Email: 2844672291@qq.com)

Yifeng Hai Pursuing a Bachelor's degree at Sichuan University of Science & Engineering. (Email: 22301030105@stu.suse.edu.cn)

Miao Zhang Pursuing a Bachelor's degree at Sichuan University of Science & Engineering. (Email: 23301030330@stu.suse.edu.cn)

Hang Chen Pursuing a Bachelor's degree at Sichuan University of Science & Engineering. (Email: 22301030101@stu.suse.edu.cn)